Ivan Shelaev, Michael Gorka, Anton Savitsky*, Vasily Kurashov,
Mahir Mamedov, Fedor Gostev, Klaus Möbius*,
Victor Nadtochenko*, John Golbeck* and Alexey Semenov*

Effect of Dehydrated Trehalose Matrix on the Kinetics of Forward Electron Transfer Reactions in Photosystem I

Abstract: The effect of dehydration on the kinetics of forward electron transfer (ET) has been studied in cyanobacterial photosystem I (PS I) complexes in a trehalose glassy matrix by time-resolved optical and EPR spectroscopies in the 100 fs to 1 ms time domain. The kinetics of the flash-induced absorption changes in the subnanosecond time domain due to primary and secondary charge separation steps were monitored by pump–probe laser spectroscopy with 20-fs low-energy pump pulses centered at 720 nm. The back-reaction kinetics of P_{700} were measured by high-field time-resolved EPR spectroscopy and the forward kinetics of $A_{1A}^{\bullet-} / A_{1B}^{\bullet-} \rightarrow F_X$ by time-resolved optical spectroscopy at 480 nm. The kinetics of the primary ET reactions to form the primary $P_{700}^{\bullet+} A_0^{\bullet-}$ and the secondary $P_{700}^{\bullet+} A_1^{\bullet-}$

---

*Corresponding authors: Anton Savitsky, Max Planck Institute for Chemical Energy Conversion, Stiftstrasse 34-36, 45470 Mülheim an der Ruhr, Germany, Phone: 0049-208-3063555, Fax: 0049-208-3063955, e-mail: anton.savitsky@cec.mpg.de;

Klaus Möbius, Max-Planck-Institut für Chemische Energiekonversion, Stiftstr. 34-36, D-45470 Mülheim an der Ruhr, Germany; and Fachbereich Physik, Freie Universität Berlin, Arnimallee 14, D-14195 Berlin, Germany, e-mail: moebius@physik.fu-berlin.de;

Victor Nadtochenko, N.N. Semenov Institute of Chemical Physics, Russian Academy of Sciences, ul. Kosygina 4, 119991 Moscow, Russia, e-mail: nadtochenko@gmail.com;

John Golbeck, Department of Biochemistry and Molecular Biology, Department of Chemistry, The Pennsylvania State University, University Park, PA 16802, USA, e-mail: jhg5@psu.edu;

and **Alexey Semenov,** N.N. Semenov Institute of Chemical Physics, Russian Academy of Sciences, ul. Kosygina 4, 119991 Moscow, Russia; and A.N. Belozersky Institute of Physical–Chemical Biology, Moscow State University, Moscow, Leninskie Gory, Moscow 119992, Russia, e-mail: semenov@genebee.msu.ru

Ivan Shelaev and Fedor Gostev: N.N. Semenov Institute of Chemical Physics, Russian Academy of Sciences, ul. Kosygina 4, 119991 Moscow, Russia

Michael Gorka and Vasily Kurashov: Department of Biochemistry and Molecular Biology, The Pennsylvania State University, University Park, PA 16802, USA

Mahir Mamedov: A.N. Belozersky Institute of Physical–Chemical Biology, Moscow State University, Moscow, Leninskie Gory, Moscow 119992, Russia

ion radical pairs were not affected by dehydration in the trehalose matrix, while the yield of the $P_{700}^{\bullet+}A_1^{\bullet-}$ was decreased by ~20%. Forward ET from the phylloquinone molecules in the $A_{1A}^{\bullet-}$ and $A_{1B}^{\bullet-}$ sites to the iron–sulfur cluster F_X slowed from ~220 ns and ~20 ns in solution to ~13 μs and ~80 ns, respectively. However, as shown by EPR spectroscopy, the ~15 μs kinetic phase also contains a small contribution from the recombination between $A_{1B}^{\bullet-}$ and $P_{700}^{\bullet+}$. These data reveal that the initial ET reactions from P_{700} to secondary phylloquinone acceptors in the A- and B-branches of cofactors (A_{1A} and A_{1B}) remain unaffected whereas ET beyond A_{1A} and A_{1B} is slowed or prevented by constrained protein dynamics due to the dry trehalose glass matrix.

Keywords: electron transfer; EPR; optical spectroscopy; photosystem I; trehalose matrix.

1 Introduction

Photosystem I (PS I) from cyanobacteria, algae, and higher plants is a chlorophyll (Chl)-protein complex that contains low-potential iron-sulfur clusters (F_A/F_B), which act as terminal electron acceptors. PS I belongs to the Type I class of photosynthetic reaction centers (RCs) and is evolutionarily close to the RCs of green sulfur bacteria and heliobacteria [1]. PS I is responsible for light-induced electron transfer (ET) from plastocyanin to ferredoxin, although, in cyanobacteria, cytochrome c_6 and flavodoxin function as alternative donor and acceptor, respectively. The three-dimensional structure of PS I from the thermophilic cyanobacterium *Thermosynechococcus elongatus* has been solved by X-ray crystallography at a resolution of 2.5 Å [2]. Each monomer (~300 kDa) contains one copy of 12 different proteins. The membrane-spanning core consists of two large subunits (products of genes *psaA* and *psaB*), which bind most of the chlorophyll (Chl) *a* molecules, 22 β-carotene molecules, two phylloquinone molecules, and an interpolypeptide [4Fe–4S] cluster named F_X. The majority of the 96 Chl *a* molecules function as light-harvesting antenna. The terminal [4Fe–4S] clusters, F_A/F_B, are bound to the peripheral stromal subunit PsaC, which has a molecular mass of ~9 kDa.

The membrane embedded core of each PS I monomer is formed by the two largest subunits, PsaA and PsaB, which bind ET cofactors arranged in two symmetrical branches termed A and B. The ET cofactors extend from P_{700}, a pair of Chl *a* molecules located on the lumenal side, to the interpolypeptide [4Fe–4S] cluster F_X, located on the opposite stromal side of the monomer. Each of the two branches are related by a pseudo-C_2 rotation axis, which passes through P_{700} and F_X, and

includes two Chl *a* molecules (termed A_{0A} or A_{0B}) and one phylloquinone (A_{1A} or A_{1B}). At room temperature (RT) both branches are active in ET [3] (for review see [4, 5]) with a ratio of ~ 80 : 20% in favor of branch A in cyanobacterial PS I [6–8]. The degree of involvement of the A and B branches in ET from prokaryotic and eukaryotic photosynthesizing organisms still remains a matter of debate.

The primary charge separation step in PS I involves ET from the excited special pair of Chl molecules P_{700}^* to the primary Chl acceptor A_{0A}/A_{0B}, with the formation of the primary ion-radical pair $P_{700}^{\bullet+}A_0^{\bullet-}$. The subsequent steps include ET from A_{0A}/A_{0B} to the phylloquinone acceptor A_{1A}/A_{1B} and to the iron-sulfur clusters F_X, F_A and F_B.

It has been shown that upon preferential excitation of P_{700}, the formation of the $P_{700}^{\bullet+}A_0^{\bullet-}$ charge-separated state is complete within 100 fs [9]. The lifetime of the subsequent ET step with the formation of the secondary ion-radical pair $P_{700}^{\bullet+}A_1^{\bullet-}$ is within 13 ps to 26 ps [9, 10]. The forward ET from $A_{1A}^{\bullet-}$ and $A_{1B}^{\bullet-}$ to F_X occurs with lifetimes of 200–300 ns and 15–25 ns, respectively [5, 11, 12]. The former reaction from $A_{1A}^{\bullet-}$ to F_X has an activation energy of 110 meV, while the latter reaction is nearly temperature independent [6, 13].

In the absence of exogenous acceptors, the electron on $(F_A/F_B)^-$ recombines with $P_{700}^{\bullet+}$ with lifetimes of 30–100 ms, while charge recombination from F_X^- occurs within 0.5–5 ms. The back-reactions between $P_{700}^{\bullet+}A_{1A}^{\bullet-}$ and $P_{700}^{\bullet+}A_{1B}^{\bullet-}$ take place within ~ 100–200 μs and 10–20 μs, respectively [4, 5, 14, 15].

During the last few decades, sugar-glass matrices have attracted a growing interest in the biotechnology community for their ability to stabilize labile proteins, including therapeutic polypeptides, and to optimize their storage at RT in the solid state [16–19]. Among other saccharides, trehalose (α-D-glucopyranosyl α-D-glucopyranoside) forms, upon dehydration at RT, glassy matrices that protect the hosted protein against denaturation induced by freezing, heating, and drying. In nature, the bioprotective action of trehalose and other disaccharide glasses is used by several organisms, allowing survival for long periods (up to years) of extreme draught and high temperatures by preserving the integrity of their cellular structures, while reversibly arresting their metabolism ("anhydro-biosis") [20, 21].

In previous years, Venturoli and coworkers have extensively used the incorporation of proteins into trehalose glasses to investigate the role of internal protein dynamics in long-range ET within bacterial photosynthetic reaction centers (bRCs) [22–25]. This integral pigment-protein complex represents one of the simplest photosystems capable of catalyzing the primary events of photosynthetic energy transduction. Hence, the bRC is often used as a model complex suitable for elucidating light-induced electron-transfer processes in the more complex RCs of oxygenic photosynthesis. It was shown that a progressive dehydration of the

trehalose-bRC glass below ~ 0.07 g of water per g of dry matrix first affects ET from the photoreduced primary quinone acceptor $Q_A^{\cdot-}$ to the secondary quinone acceptor Q_B, causing a block in an increasing fraction of the bRC population up to a complete arresting of light-induced ET over the whole bRC population at RT. This effect is similar to what is observed in water-glycerol mixtures at temperatures below 200 K [24]. The authors ascribed the reversible inhibition of ET to Q_B in the trehalose glass to a large increase of the energy barriers between conformational substates that govern the transition probability for gated ET. On further dehydration (below ~ 0.03 g of water per g of dry matrix) the kinetics of $P_{865}^{\cdot+}Q_A^{\cdot-}$ recombination abruptly increased and became broadly distributed, mimicking at RT the kinetics observed at cryogenic temperatures (T < 100 K) in a glycerol-water mixture [22, 24, 25]. This similarity indicates that in bRCs embedded in extremely dehydrated trehalose matrices thermal fluctuations between conformational substates, as well as relaxation from the dark-adapted to the light-adapted conformation [26, 27], are largely hindered at RT over the timescale of 10^{-1} s. It was proposed that a network of hydrogen bonds, involving residual water molecules, connects the protein surface to the trehalose matrix, thereby determining a tight structural and dynamical coupling between the bRC and the stiff water-sugar matrix [23, 28, 29].

Recently, the coupling between light-induced ET and protein-solvent dynamics in PS I was studied at RT by incorporating this large protein complex into trehalose glasses at different hydration levels [30]. It was demonstrated that functional PS I complexes can be embedded into a structurally and dynamically homogeneous trehalose matrix without distorting the molecular configuration of the $P_{700}^{\cdot+}A_1^{\cdot-}$ radical pair. The kinetics of charge recombination after a pulsed excitation, probed by time-resolved EPR and optical NIR absorption spectroscopy, was studied as a function of the hydration level of the trehalose matrix. It was shown that dehydration below 0.11 g of water per g of dry matrix blocks forward ET beyond F_X. Below ~ 0.07 g of water per g of dry matrix, ET from $A_1^{\cdot-}$ to F_X also becomes hindered in a significant fraction of PS I. However, the effect of dry trehalose matrix on the kinetics of forward ET has not been studied. Moreover, the possible effect of dry trehalose glass on the fast charge recombination kinetics has not yet been tested, largely because the time resolution of the flash-induced $P_{700}^{\cdot+}$ reduction measured at 820 nm in our previous work was restricted to ~ 10 μs [30]. Dehydration at RT mimicked the effects of freezing water-glycerol PS I systems [31], suggesting an impairment of PS I protein dynamics in the dry trehalose glass.

In the present work, femtosecond pump–probe spectroscopy in the time domain from 100 fs to 600 ps and time-resolved absorption spectrometry at 480 nm with time resolution >10 ns were used to investigate the effect of

disaccharide trehalose glassy matrix on the forward electron-transfer kinetics of the formation of primary and secondary ion-radical pairs, as well as on ET from $A_1^{\cdot-}$ to the iron–sulfur centers in both the A and B branches. In addition, the effect of trehalose on charge recombination kinetics in the time domain of 2–70 µs was determined using a pulse high-frequency EPR spectroscopy at 95 GHz.

2 Materials and methods

2.1 Cell growth and isolation of PS I complexes

A glucose-tolerant strain of *Synechocystis* sp. PCC 6803 was grown at 30°C in BG-11 medium under light. Cyanobacterial cultures in late exponential phase were pelleted by centrifugation, washed twice with BG-11 medium, and suspended in 50 mM Tris-HCl buffer (pH 8.1). PS I trimeric complexes were isolated using *n*-dodecyl-β-D-maltoside (DM) and sucrose gradients as described earlier [32]. The isolated PS I preparation was resuspended in 50 mM Tris-HCl buffer (pH 8.1) containing 0.03% (w/v) DM, frozen as small aliquots at a Chl *a* concentration of 2 mg mL^{-1} in liquid nitrogen, and stored at − 90°C. Chlorophyll was extracted from PS I trimers with 80% acetone and determined as described in [33].

2.2 Preparation of trehalose-PS I glassy matrices

Trehalose-PS I glassy matrices were prepared following the procedure for the incorporation of bacterial RCs and PS I into trehalose glasses [30, 34]. For measuring the kinetics of $P_{700}^{\cdot+}$ decay after a laser pulse, trehalose-PS I glasses were prepared from a 30−40 µL drop of an aqueous solution of 50 mM Tris-HCl, pH 7.5, 0.03% (w/v) DM, 782 mM trehalose, and PS I corresponding to a final Chl *a* concentration of 1.1 mM. This yielded a trehalose/PS I trimer molar ratio of $2.0 \cdot 10^5$. Vitrification was carried out by drying at RT the trehalose-PS I liquid drop, deposited on a glass slide, under N$_2$ flow inside a desiccator for about 4 h, as described in [35]. The optical window on which the solid amorphous sample was formed, was exposed to the 11% of relative humidity by placing it inside a gastight sample holder, containing at the bottom about 1.5 mL of the saturated solution of LiCl [36]. W-band and X-band EPR were performed on trehalose-PS I samples characterized by a trehalose/PS I trimer molar ratio of $4.0 \cdot 10^4$ obtained from a drop containing 545 mM trehalose and 1.5 mM PS I Chl *a*. To maintain the primary electron donor pre-reduced during the vitrification process, 5 mM Na-ascorbate and 5 µM

2,6-dichlorophenol-indophenol (DCPIP) were added to all these liquid samples. X-band EPR spectra of aqueous-solution samples were measured at a concentration of 0.5 mg/mL Chl pretreated with 1 mM sodium ascorbate and dark-adapted for 45 min, then frozen in the dark with liquid nitrogen.

2.3 Femtosecond laser photolysis

Transient absorption spectra were measured using a femtosecond pump to supercontinuum probe setup. The output of a Ti : sapphire oscillator (800 nm, 80 MHz, 80 fs, Tsunami, Spectra-Physics) was amplified by a regenerative amplifier system (Spitfire, Spectra-Physics, USA) at a repetition rate of 1 kHz as described earlier. The amplified pulses were split into two beams. One of the beams was directed into a noncollinearly phase-matched optical parametric amplifier. Its output, centered at 710 nm, was compressed by a pair of quartz prisms. The Gauss pulse of 22 fs at 720 nm was used as the pump. The second beam was focused onto a thin quartz cell with H_2O to generate supercontinuum probe pulses. The pump and probe pulses were time delayed with respect to each other using a computer-controlled delay stage. They were then attenuated, recombined, and focused onto the sample cell. The pump and probe light spots had diameters of 300 µm and 120 µm, respectively. The pump pulse energy was attenuated at 20 nJ to achieve optimal excitation with an average number of excitons per one PS I of close to 0.1. This means that PS I excited with multiexcitons can be neglected. Experiments were carried out at 278 K. Frequency control of the laser pulses was produced by regular device synchronization using control amplifier SDG II Spitfire 9132, manufactured by Spectra Physics (USA). The device allowed one to change the pulse repetition frequency of the amplifier output from 0 to 1000 Hz. The pump pulse operation frequency was 10 Hz, which is sufficiently low to exclude permanent bleaching due to photochemical processes in the sample. The relative polarizations of pump and probe beams were adjusted to 54.7° (magic angle). After passing the sample, the supercontinuum was dispersed by a polychromator (Acton SP-300) and detected by a CCD camera (Roper Scientific SPEC-10). Transient spectra of absorbance changes $\Delta A(t, \lambda)$ were recorded over the range of 380–800 nm. The measured spectra were corrected for group delay dispersion of the supercontinuum using the procedure described previously [37, 38]. Particular attention was given to the "coherence spike"' or "coherent artifact" that is observed at the beginning of the measurement during pump–probe overlap and prevents the analysis of measurements at delays < 70 fs. The problem of the resonant signal of the chromophore molecule in solution for the "coherent artifact" time window was analyzed according to [39].

2.4 Time-resolved optical studies at 480 nm

The kinetics of phylloquinone oxidation were measured by monitoring transient absorbance changes at 480 nm following a single-turnover laser flash at 532 nm using a laboratory-built, dual-beam spectrometer as described previously [6]. The measuring beam was provided by a 480 laser diode (OptoEngine MBL-H-480-30 mW) that was passed through a beam expander (Thorlabs BE05M-A) to a diameter of 1 cm and controlled by a mechanical shutter that opened 2 ms prior to the actinic flash. Liquid samples were placed in a 10 mm×10 mm quartz cuvette and contained 50 μg/mL Chl, Tris-HCl (pH 8.3), 10 μM DCPIP, 5 mM sodium ascorbate, and 0.05% (w/v) DM. Glass samples were placed perpendicular to the probe beam, and the actinic beam illuminated the sample face at a 45-degree angle. It is important to note that glass samples were not measured for a duration of more than 1 h to prevent rehydration. The measuring and reference beam intensities were balanced using a variable density optical filter wheel. The difference signal was amplified with a differential amplifier (Thor Labs PDB460A) and processed using a 12-bit, 200 MS/s, NI-5124 PCI card (National Instruments). The data acquisition was controlled using software written in LabView (National Instruments), and the time course was analyzed using CONTIN program [40]. In the analysis of recombination kinetics, we have used the CONTIN algorithm, because it does not require any *a priori* assumption on the number of "discrete lifetimes" or continuous, distributed kinetic components. The solution of complex kinetics obtained by CONTIN analysis is unique.

2.5 W-band EPR measurements

The EPR sample was prepared using small fragments of dry trehalose-PS I glass with a trehalose/ PS I (trimer) molar ratio of $4 \cdot 10^4$. They were placed into the cylindrical quartz capillaries (0.6 mm I.D.) for the W-band EPR cavity. In order to equilibrate the EPR sample at 11% relative humidity, a drop of saturated LiCl aqueous solution was inserted into the capillary. It was then sealed and equilibrated for 1 week before the measurements, as described in [34]. W-band EPR measurements were performed using a laboratory-built spectrometer operating at a microwave (MW) frequency of 95 GHz and an external magnetic field B_0 of 3.4 T. The spectrometer is optimized for continuous wave (CW) and pulse experiments, as described previously [41]. For optical sample irradiation the light was guided to the center of the cavity through a quartz fiber of 0.8 mm diameter. The ET was initiated by singlet excitation of the primary donor P_{700} at 532 nm using a frequency-doubled Nd:YAG laser (5 ns pulse length, 1–10 Hz repetition rate, 0.5 mJ/pulse on the sample surface) or CW diode laser (690 nm, 40 mW). The transient EPR signals were acquired employing the MW pulse sequence for primary electron spin-echo

(ESE) generation. It was applied at the time, T_{DAF}, after pulsed laser excitation: $h\nu$-T_{DAF}-$(t_p)_{x,-x}$-τ-$(2t_p)$-τ-echo. The pulse length t_p of the $\pi/2$ MW pulses was generally set to 30 ns. For field-swept ESE detected spectra the pulse separation time τ was fixed to 150 ns. To characterize the $P_{700}^{\bullet+}A_1^{\bullet-}$ charge-recombination the echo decay traces were obtained at the fixed magnetic field position corresponding to the maximum of the $P_{700}^{\bullet+}$ EPR absorption signal when varying T_{DAF}.

2.6 X-band EPR measurements

X-band time/field transient EPR data sets were measured using a modified ESP 300E spectrometer equipped with an ER 042 MRH X-band microwave bridge and a Flexline ER 4118 X-MD-5W1 dielectric resonator (Bruker BioSpin). Single-turnover flashes were supplied by a Vibrant 355II laser (Opotek) running at 10 Hz and a wavelength of 532 nm at 20 mJ per pulse. The temperature was controlled using a CF935 continuous flow cryostat (Oxford Instruments). The transient EPR signal was collected in direct-detection mode with a home-built broadband amplifier (bandwidth > 500 MHz). The signal was digitized using a 500 MHz bandwidth, 8-bit, 2GS/s, Model CS85G PCI card (GaGe Instruments). The software for data acquisition was written in-house using LabView (National Instruments). The data was analyzed using IGOR software (Wavemetrics).

X-band CW EPR experiments were carried out using an ELEXSYS EPR spectrometer equipped with a Super X CW-EPR microwave bridge and a high-Q resonator (Bruker BioSpin). The sample was cooled using an ESR 900 cryostat (Oxford Instruments). A Coherent Verdi-V5 laser (1 W at 532 nm) provided the excitation and was passed through a three-fold beam expander (Oriel Instruments) before entering the resonator.

3 Results and discussion

3.1 Pump–probe ultrafast measurements

In a previous paper, we used a complex approach to study the primary reactions in PS I, including short (~ 20 fs) flashes centered at 720 nm with a bandwidth of 40 nm (fwhm), which allowed predominant excitation of the PS I primary electron donor, the Chl dimer P_{700} [9]. Low energy pulses (20 nJ) provided excitation at the one-exciton level. As was previously shown, under our experimental conditions we observed very fast (< 100 fs) charge separation with formation of the $P_{700}^{\bullet+}A_0^{\bullet-}A_1$ state in approximately one half of RCs, and the ~ 5-ps energy transfer

from antenna Chl* to $P_{700}A_0A_1$ in the remaining fraction of RCs. These conditions were chosen to maximize the relative contribution of the direct excitation of the RC in order to discriminate between the kinetics of primary stages of charge separation from the kinetics of excitation energy transfer in the antenna. Based on this approach, it was possible to reveal the difference spectra of the intermediates, $(P_{700}A_0)^*$, $P_{700}^{\bullet+}A_0^{\bullet-}$ and $P_{700}^{\bullet+}A_1^{\bullet-}$, and to describe the kinetics of transitions between these intermediates.

Figure 1 shows transient spectra, $\Delta A(\lambda, t)$, of PS I embedded in the trehalose glassy matrix at 11% relative humidity (ΔA_{tr}) obtained upon excitation by a 720 nm 20 fs pulse at different time delays. The differential spectra at an early delay reveal bleaching in the Soret and Q_y bands and excited state absorption (ESA) in the range of 460–540 nm and around 660 nm. ESA can be due both to the absorption of electronically excited Chl molecules and to the appearance of the Chl-cation and Chl-anion radicals due to ET between redox cofactors. The spectrum represents the superposition of Chl excited state properties and features previously assigned to $P_{700}/P_{700}^{\bullet+}$ and $A_0/A_0^{\bullet-}$ differential spectra [42–45]. The two bleaching peaks in the Q_y band at 690 and 705 nm, which appear at the shortest time delay (~ 70 fs), were earlier ascribed to the ultrafast formation of the primary ion-radical pair $P_{700}^{\bullet+}A_0^{\bullet-}$; subsequent formation of the secondary ion-radical pair $P_{700}^{\bullet+}A_1^{\bullet-}$ (the spectral evolution at later time delays in Figure 1) has a characteristic time of ~ 25 ps [9].

The differential spectra recorded at different time delays and the positions of the absorption changes are similar for PS I embedded into dry trehalose glassy matrix (this paper) and for PS I in solution in the presence of detergent [9].
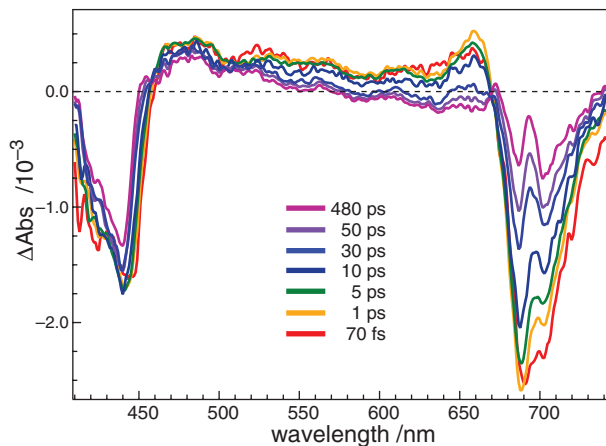

Fig. 1: Transient spectra of PS I embedded in the glassy matrix at 11% humidity recorded at different time delays between pump and probe pulses at 290 K.

Figure 2 shows a comparison of the PS I transient spectra in the trehalose glassy matrix and in solution at early (Figure 2a, 120 fs) and late (Figure 2b, 480 ps) time delays after the pump laser flash. As indicated earlier, the spectrum recorded at a time delay of ~100 fs has the spectral features of the primary ion-radical pair $P_{700}^{\bullet+}A_0^{\bullet-}$. These specific features include the bleaching at ~690 nm corresponding to the $A_0 \to A_0^{\bullet-}$ transition and the bleaching at 705 nm due to formation of $P_{700}^{\bullet+}$, while the spectrum at a later time delay can be safely ascribed to the secondary ion-radical pair $P_{700}^{\bullet+}A_1^{\bullet-}$ [9]. The transient spectra shown in Figure 2a at 120 fs delay are similar for PS I in solution (trace 2) and in the trehalose glassy matrix (trace 1). The qualitative similarity of the transient spectral shape at short and long time delays for PS I in trehalose and in solution suggests a similar mechanism of primary charge separation. It also suggests the ultrafast formation of the $P_{700}^{\bullet+}A_0^{\bullet-}$ state in both systems. However, quantitative analysis reveals some difference in the transient spectra at long delays for PS I in trehalose and in solution. The spectra shown in Figure 2b for PS I in solution (trace 2) and in trehalose (trace 1) at a time delay of 480 ps differ in the amplitude of the peaks at 690 nm, 450 nm and 675 nm. These peaks are typical for the formation of the $P_{700}^{\bullet+}A_1^{\bullet-}$ radical pair. The lower amplitude of these peaks in the trehalose glassy matrix suggests a lower yield of the $P_{700}^{\bullet+}A_1^{\bullet-}$ radical pair.

To determine the ET rate for the $P_{700}^{\bullet+}A_0^{\bullet-}$ to $P_{700}^{\bullet+}A_1^{\bullet-}$ transition in the trehalose glassy matrix we performed a global analysis of the experimental data $\Delta A(\lambda, t)$,
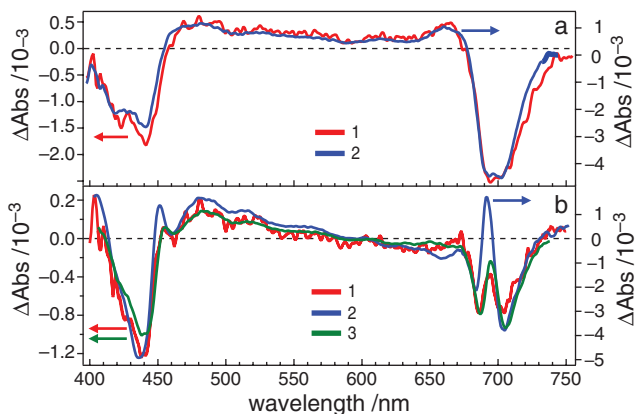

Fig. 2: Transient spectra of PS I in trehalose and in solution at different time delays after the pump laser flash at 290 K. (a) time delay of 120 fs; 1 – transient spectrum of PS I in the trehalose glassy matrix; 2 – transient spectrum of PS I in solution. (b) Time delay of 480 ps; 1 – transient spectrum in the trehalose glassy matrix; 2 – experimental transient spectrum in solution; 3 – transient spectrum calculated as the linear composition of transient spectra of PS I in solution according to Eqs. (1–2). The corresponding y-axes for each trace are marked by arrows.

suggesting that the differential spectrum at 480 ps delay corresponds to the spectrum of $P_{700}^{\bullet+}A_1^{\bullet-}$ state. The principal component analysis [46] of the data matrix used to estimate the rate of the $P_{700}^{\bullet+}A_0^{\bullet-}$ to $P_{700}^{\bullet+}A_1^{\bullet-}$ transition revealed the rate constant of the main component kinetics of $k = 0.037 \pm 0.0014$ ps^{-1}, which corresponds to a lifetime of $\tau \sim 27$ ps.

To explain the difference in the spectra at the 480 ps delay time, we suggest that the spectrum in the trehalose glassy matrix (ΔA_{tr}) is the superposition of two spectra in solution (ΔA_{sol}) typical for the primary ion-radical pair $P_{700}^{\bullet+}A_0^{\bullet-}$ at 120 fs and for the secondary ion-radical pair $P_{700}^{\bullet+}A_1^{\bullet-}$ at 480 ps delay:

$$\Delta A_{tr}(480 \text{ ps}) = c_1 \times \Delta A_{sol}(120 \text{ fs}) + c_2 \times \Delta A_{sol}(480 \text{ ps}) \qquad (1)$$

The coefficients c_1 and c_2 in equation (1) were determined by χ^2 minimization with regard to the combination of the experimental spectra. The ratio of coefficients was estimated as:

$$c_1/(c_1 + c_2) = 0.22 \pm 0.03 \text{ and } c_2/(c_1 + c_2) = 0.78 \pm 0.06 \qquad (2)$$

Figure 2b shows the experimentally-measured spectra, $\Delta A_{tr}(480 \text{ ps})$ (trace 1) and $\Delta A_{sol}(480 \text{ ps})$ (trace 2), and the resulting spectrum $c_1 \times \Delta A_{sol}(120 \text{ fs}) + c_2 \times \Delta A_{sol}$ (480 ps) with the calculated c_1 and c_2 values (trace 3). The similarity between traces 1 and 3 suggests that the formation of the secondary ion-radical pair $P_{700}^{\bullet+}A_1^{\bullet-}$ in the trehalose glassy matrix at the 480 ps delay time is achieved in ~80% of PS I. We propose that in the remaining ~20% of PS I, the photooxidized primary donor $P_{700}^{\bullet+}$ recombines with the primary acceptor $A_0^{\bullet-}$, thus preventing forward ET in this fraction of the PS I complexes.

These results show that incorporation of the PS I complex into the trehalose glassy matrix at low hydration levels does not affect the kinetics or spectra of the primary charge separation states, i.e. the formation of the primary $P_{700}^{\bullet+}A_0^{\bullet-}$ and the secondary $P_{700}^{\bullet+}A_1^{\bullet-}$ ion-radical pairs. However, the lower yield of $P_{700}^{\bullet+}A_1^{\bullet-}$ formation in the trehalose glassy matrix suggests a partial prevention of the $P_{700}^{\bullet+}A_0^{\bullet-}$ to $P_{700}^{\bullet+}A_1^{\bullet-}$ transition in a small fraction of PS I. This effect can be rationalized by a partial extrusion of tightly bound water molecules from the intraprotein pool located between the A_1 and F_X-binding sites as was suggested in [30].

3.2 Time-resolved optical measurements at 480 nm

Measurements at 480 nm monitor the electrochromic bandshift of a carotenoid near the A_{1A} or A_{1B} sites that occurs upon phylloquinone reduction [31]. Although indirect, this makes it possible to measure the transient redox changes of any quinone occupying the A_{1A} and A_{1B} binding sites after excitation. It should be

noted that while the majority of the signal is a result of phylloquinone reduction/reoxidation, $P_{700}^{\bullet+}$ also absorbs in this region and constitutes about 1/3 of the total signal. Additionally, due to the actinic effect of the measuring probe beam, samples are only measured to 400 µs, and any kinetic phases thereafter are an artifact of the fitting software [6].

The kinetics measured at 480 nm for WT PS I in solution are shown in Figure 3a and the CONTIN deconvolution is shown in Figure 3b (green line). The lifetimes of the kinetic phases and their relative amplitudes are listed in Table 1.
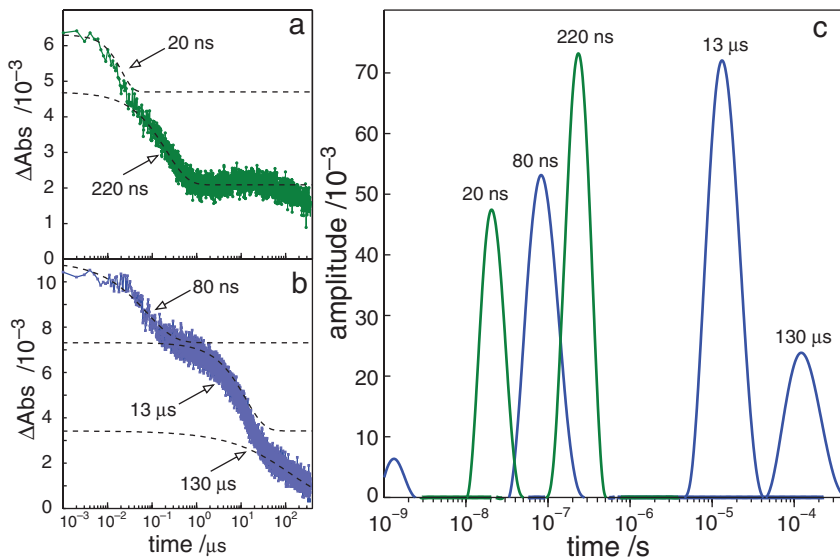

Fig. 3: Time-resolved optical spectra at 480 nm recorded at 290 K for WT PS I in solution (a), and in trehalose (b). (c) The CONTIN deconvolution of the solution sample (green line) and trehalose sample (blue line) is shown on the right with peaks corresponding to the lifetimes. The CONTIN data was subsequently used to deconvolute the original traces into individual kinetic phases shown by dashed lines in panels (a) and (b). Note: the samples were only measured to 400 µs.

Tab. 1: Lifetimes (τ) and relative amplitudes of the kinetic phases measured at 480 nm for PS I in solution and in trehalose.

Solution				
τ	20 ns	220 ns		Long-lived components
Amplitude	23%	40%		37%
Trehalose				
τ	80 ns	13 µs	130 µs	Long-lived components
Amplitude	32%	44%	15%	8%

We observe two major kinetic phases with lifetimes of 20 ns and 220 ns in a ratio of 1 : 1.74 (fast : slow). These phases have been well characterized [3, 47] and are assigned to ET from to $A_{1A}^{\bullet-}$ F_X (~220 ns) and $A_{1B}^{\bullet-}$ to F_X (~ 20 ns), respectively; the remaining portion of the spectra that has not decayed on this timescale (37% of the total signal) is due to the absorbance of $P_{700}^{\bullet+}$.

The kinetics measured at 480 nm for WT PS I in the trehalose glassy matrix are shown in Figure 3b and the CONTIN deconvolution is shown in Figure 3c (blue line). Several differences are readily apparent when compared to PS I in solution. The kinetic phases with lifetimes of 20 ns and 220 ns are absent and instead kinetic phases with lifetimes of 80 ns and a 13 µs are present in a roughly 1 : 1.4 ratio. In addition, we observe the onset of a 130 µs kinetic phase that does not fully decay to the baseline in 400 µs. A similar phase was observed in the kinetics of $P_{700}^{\bullet+}$ recombination measured at 820 nm in dry trehalose matrix [30] and was ascribed to the $A_{1A}^{\bullet-} \rightarrow P_{700}^{\bullet+}$ back reaction. Therefore we suggest that $P_{700}^{\bullet+}A_{1A}^{\bullet-}$ recombines in ~15% of PS I under the conditions of our experiment. Approximately 8% of the signal has not decayed at the end of the measuring period and is attributed to $P_{700}^{\bullet+}$.

To assign these phases to the various possible routes of phylloquinone oxidation, we examine the experimentally determined lifetimes for $A_{1A}^{\bullet-}$ and $A_{1B}^{\bullet-}$ to F_X ET reported previously at low temperature. In studies carried out by Agalarov and Brettel [13] the forward rate of ET from $A_{1A}^{\bullet-}$ and $A_{1B}^{\bullet-}$ at low temperature in 65% glycerol glass was measured as a function of sample temperature, and activation energies were determined using the Arrhenius equation:

$$k = A \cdot e^{-E_a/RT} \qquad (3)$$

where k is the rate in units of s^{-1}, E_a is the activation energy, and T is the absolute temperature in Kelvin. The activation energies for the fast and slow phases were found to be 15 meV and 110 meV, respectively.

Knowing the activation energy and using Eq (3), we can calculate the temperature at which forward ET from $A_{1A}^{\bullet-}$ and $A_{1B}^{\bullet-}$ to F_X in a 65% glycerol glassy matrix would have the same lifetime as in trehalose at RT. Using a value of 110 meV for the activation energy, the slow kinetic phase ($A_{1A}^{\bullet-}$ to F_X) would have a lifetime of 13 µs at a temperature of 152 K. This is close to the glass transition temperature of 65% glycerol in water, which is 167 K. Similarly, using a value of 15 meV for the activation energy, the fast kinetic phase ($A_{1B}^{\bullet-}$ to F_X) would have a lifetime of 80 ns at a temperature of 89 K. The latter is considerably below the glass transition temperature of 65% glycerol in water, however, determination of activation energies of these processes are subject to a reasonably high degree of imprecision. It should be noted in an earlier study by [31] the activation energy for the slow kinetic phase was estimated to be 220 mV. Inverting the argument, the activation energy that

would yield a lifetime of 80 ns at a temperature of 167 K would be 46 meV (similarly, the activation energy that would yield a lifetime of 13 µs at a temperature of 167 K would be 135 meV). Further, as was mentioned in Section 1 of the Results, the ultrafast pump–probe measurements suggest that in the trehalose glassy matrix, the photooxidized primary donor $P_{700}^{\bullet+}$ recombines with the primary acceptor $A_0^{\bullet-}$ in ~ 20% of PS I, thus preventing forward ET. The lifetime of $P_{700}^{\bullet+}A_0^{\bullet-}$ recombination is in the range of tens of nanoseconds [6, 48]. Therefore, the 80 ns phase can be due to the superposition of the $A_{1B}^{\bullet-}$ to F_X forward reaction and the $A_0^{\bullet-}$ to $P_{700}^{\bullet+}$ back reaction, which occur in a similar time range, and which may not be distinguishable by our deconvolution routine. In this case, the exact lifetime of the forward ET cannot be estimated accurately, and hence the estimation of the activation energy for the fast kinetic phase would represent an upper limit.

Work by [30] reported a kinetic phase with a lifetime of ~ 100 µs for PS I in dry trehalose glassy matrix and attributed this kinetic phase to charge recombination with $P_{700}^{\bullet+}$. Thus we propose that the observed 130 µs phase arises from a population of $A_{1A}^{\bullet-}$ that recombines with $P_{700}^{\bullet+}$. The 13 µs phase is not only due to forward ET from $A_{1A}^{\bullet-}$ to F_X, but according to Section 3 (see below) is also partially due to back reaction from $A_{1B}^{\bullet-}$ to $P_{700}^{\bullet+}$. That means both the 13 µs and 130 µs kinetic phases have contributions from both $P_{700}^{\bullet+}$ and $A_{1A}^{\bullet-}$.

3.3 W-band EPR measurements

The lifetime of two key ET cofactors in PS I, the primary donor cation radical of $P_{700}^{\bullet+}$ and the quinone acceptor anion radical of $A_1^{\bullet-}$, can be probed by examining the time changes in the EPR spectrum of the radical pair. Immediately after the laser flash, the $P_{700}^{\bullet+}A_1^{\bullet-}$ radical pair is created in the pure singlet electronic state leading to the appearance of a spin-polarized EPR spectrum, see Figure 4a (lower trace). This type of electron-spin polarization phenomenon is well described by the correlated-coupled radical-pair (CCRP) model [49–55].

In solid amorphous samples, the transient EPR lineshape, determined by the magnitude and sign of the dipolar coupling of the two electron spins, is sensitive to the relative orientation and distance of the radical-pair partners. Electron-spin polarization is observable by transient EPR with lines in emission and enhanced absorption, provided the lifetime of the radical pair and/or the electron spin-lattice relaxation times, T_1, of the individual pair partners are long enough compared to the EPR detection time [54]. The electron-spin lattice relaxation processes lead to Boltzmann thermal equilibrium of the spin populations with all lines in absorption. In the case in which the spin relaxation is faster than $P_{700}^{\bullet+}A_1^{\bullet-}$ charge recombination or subsequent forward ET from $A_1^{\bullet-}$ to the iron
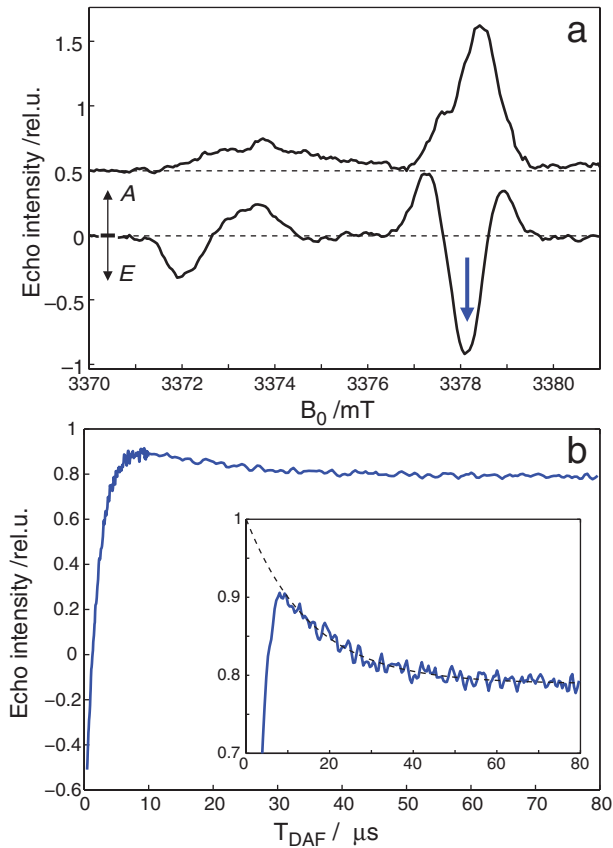
Fig. 4: (a) Field-swept echo-detected W-band EPR signals of the spin-correlated $P_{700}^{\bullet+}A_1^{\bullet-}$ radical pair in dark-adapted PS I complexes, embedded in the trehalose glassy matrix at 288 K. The spectra were recorded at $T_{DAF} = 200$ ns (lower trace) and 20 μs (upper trace) after a 532 nm laser flash using a Hahn-echo pulse sequence with $\pi/2$ pulse length of 30 ns and interpulse delay of 150 ns. Both spectra are base-line corrected using the spectrum acquired 1 μs prior to laser flash. The $A_1^{\bullet-}$ contribution to the spectrum appears at the low-field side (higher g values than the $P_{700}^{\bullet+}$ contribution). A stands for absorptive and E for emissive type of spin polarization. (b) EPR signal decay kinetics at the magnetic field position indicated by the arrow in (a). The initial signal growth corresponds to the decay of spin polarization due to spin-lattice relaxation processes. The subsequent decay is ascribed to the $P_{700}^{\bullet+}A_1^{\bullet-}$ charge recombination. The insert shows the absorption signal decay overlaid with the best-fit exponential decay (dashed line). The decay trace is normalized to the value of EPR absorption at $T_{DAF} = 0$, as obtained from simulation.

sulfur clusters, the time decay of the EPR absorption signal allows one to deduce electron-transfer rates.

Figure 4b shows the EPR signal at the B_0 value of maximum $P_{700}^{\bullet+}$ emission, see Figure 4a. The negative (emission) signal decays to the positive (absorption) signal

with a time constant of $2.0 \pm 0.2\,\mu s$. This value agrees with the spin-lattice relaxation time of $P_{700}^{\bullet+}$ $T_1 = 2.1 \pm 0.1\,\mu s$ that was determined in an inversion-recovery EPR experiment [56] using the EPR signal of $P_{700}^{\bullet+}$ generated by continuous light irradiation. The EPR spectrum acquired 20 µs after the laser flash, see Figure 4a (upper trace), does not reveal polarized spectral contributions. The spectrum shows two absorptive contributions due to $A_1^{\bullet-}$ (low field) and $P_{700}^{\bullet+}$ (high field) radicals with Boltzmann equilibrium spin populations. The decay of the thermally equilibrated $P_{700}^{\bullet+}$ signal is shown in the insert of Figure 4b. It decays with a time constant of $14 \pm 2\,\mu s$, which is in a good agreement with the $A_1^{\bullet-}$ lifetime 13.2 µs obtained from time-resolved optical measurements (see Table 1).

For a direct comparison with the results of time-resolved optical measurements, an EPR signal of $A_1^{\bullet-}$ with a good signal-to-noise ratio would be required. Unfortunately, due to the small thermally equilibrated EPR signal of $A_1^{\bullet-}$ (see Figure 4a upper trace) it was not possible to obtain decay traces with reasonable signal-to-noise ratio for accurate analysis. Additionally, the spectral contributions of thermally equilibrated $A_{1A}^{\bullet-}$ and $A_{1B}^{\bullet-}$ are not distinguishable due to very similar g-tensor values. $P_{700}^{\bullet+}$ EPR decay traces allow us to estimate the ratio of $P_{700}^{\bullet+}A_{1B}^{\bullet-}$ charge recombination to subsequent forward ET from $A_{1A}^{\bullet-}$ to F_X. Because the thermally equilibrated $P_{700}^{\bullet+}$ EPR signal decays to about 0.8 of its estimated initial value (see Figure 4b insert), further ET from $A_{1A}^{\bullet-}$ to F_X is still the dominant process and only 20% of illuminated PS I undergoes $P_{700}^{\bullet+}A_{1B}^{\bullet-}$ charge recombination. Hence, the EPR results show that ∼ 20% of the ∼ 13 µs phase observed by time-resolved optical data at 480 nm most probably reflect the recombination of $P_{700}^{\bullet+}A_{1B}^{\bullet-}$. This means that the forward ET from $A_{1A}^{\bullet-}$ to F_X is observed in ∼ 80% of PS I.

3.4 X-band EPR measurements

If, as the ultrafast optical measurements suggest, the low yield of $P_{700}^{\bullet+}A_1^{\bullet-}$ formation is due to a partial prevention of the $P_{700}^{\bullet+}A_0^{\bullet-}$ to $P_{700}^{\bullet+}A_1^{\bullet-}$ electron-transfer transition, then the recombination reaction between P_{700}^+ and A_0^- should result in the appearance of spin polarized $^3P_{700}$ signal. Figure 5a shows a transient X-band EPR spectra recorded 1 µs after the laser flash on a sample of PS I in aqueous solution (green trace) and a sample of PS I in trehalose glass at 11% humidity (blue trace) at 90 K. The sharp feature in both traces centered at 345 mT with an E/A/E polarization pattern (Figure 5a, insert) is the well-characterized $P_{700}^{\bullet+}A_1^{\bullet-}$ radical pair that results from cyclic ET along the A-branch of cofactors. The PS I sample in trehalose glass (blue trace) shows an additional set of features ascribed to the primary donor triplet state, $^3P_{700}$. In the primary donor, the Zeeman interaction in
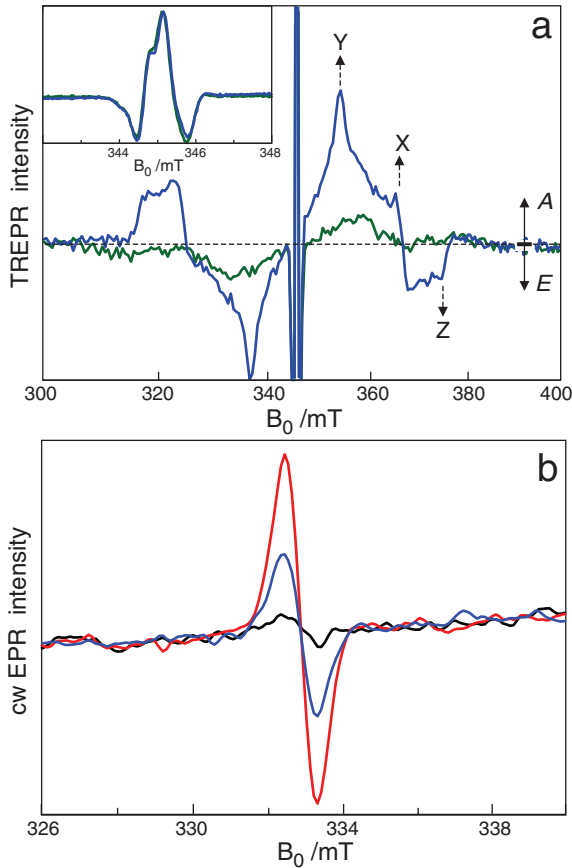
Fig. 5: (a) X-band transient EPR spectra recorded 1 μs after the laser flash for PS I in aqueous frozen solution (green), and in a trehalose glassy matrix with 11% relative humidity (blue) at 90 K. The spectra are normalized to the spin polarized $P_{700}^{\cdot+} A_1^{\cdot-}$ radical-pair signal shown in the insert on an expanded field scale. X, Y, and Z indicate the resonance positions where the static magnetic field is parallel to the principal axes of the triplet zfs tensor [57]. *A* stands for absorptive and *E* for emissive type of spin polarization. (b) X-band CW EPR spectra of PS I in a glassy trehalose matrix at 11% humidity. The black trace represents the EPR signal of a sample frozen in the dark; the red trace represents the signal of a sample during excitation by 1 W of 532 nm light; the blue trace represents the signal after cessation of illumination. Spectrometer settings: microwave power, 0.5 mW; field-modulation frequency, 100 kHz; modulation amplitude, 0.1 mT; temperature, 90 K; eight signal averages.

the external magnetic field is stronger than the electron-nuclear hyperfine interactions of typical magnitude, leading to mixing of the singlet state only with the T_0 triplet sublevel. The large Zeeman splitting of the $T_{\pm1}$ states severely limits their being mixed with the S state. Hence, here only the photochemical transformations

after light excitation with subsequent mixing of the S and T_0 states need to be considered. As a result, only the T_0 sublevel (and not the T_{+1} and T_{-1} sublevels) of the $^3P_{700}$ triplet state is populated by radical-pair recombination, leading to the characteristic A/E/E/A/A/E polarization pattern [57, 58]. In contrast, the identical PS I sample in aqueous solution (green trace) shows a very minor population of an intersystem-crossing triplet, which has a polarization pattern of E/E/E/A/A/A.

When PS I in aqueous solution is illuminated at cryogenic temperatures, about 50% of PS I remains in a $P_{700}^{\bullet+}[F_A/F_B]^{\bullet-}$ charge-separated state [59]. If, as our studies indicate, PS I in room-temperature trehalose glass partially mimics PS I in solution at the glass-transition temperature, the question arises whether a similar amount of PS I in trehalose glass, that has been exposed to light, is in the $P_{700}^{\bullet+}[F_A/F_B]^{\bullet-}$ charge-separated state at RT. To answer this question, we took a PS I preparation in trehalose glass that had been equilibrated at 11% humidity, placed it in an X-band EPR tube, and scanned the magnetic field looking for a $P_{700}^{\bullet+}$ radical signal. The sample was treated identically to those used in the optical experiments, hence it had been exposed to scattered light during sample drying and sample handling. As shown by the black trace in Figure 5b, only a small radical signal is present at $g = 2$. Its identity is uncertain, as a sample without PS I also exhibits a similar signal at the same magnetic field. When the PS I-trehalose sample is illuminated at 90 K in the resonator with 1 W of 532 nm light (red trace), a large radical signal at $g = 2$ from $P_{700}^{\bullet+}$ appears. When the light is turned off (blue trace), about 50% of the signal is retained in the charge-separated state. Thus, it appears that (i) the PS I-trehalose samples used for the room-temperature optical studies were entirely in the ground state, i.e. that very little, if any, were in the $P_{700}^{\bullet+}[F_A/F_B]^{\bullet-}$ charge-separated state, and (ii) that PS I in trehalose glass acts similarly to PS I in aqueous solution in terms of retaining ~ 50% of the reaction centers in a $P_{700}^{\bullet+}[F_A/F_B]^{\bullet-}$ charge-separated state at cryogenic temperatures after exposure to light.

4 Conclusions

The kinetics of ET reactions in PS I embedded into trehalose dry glassy matrix were studied in the time range from 100 fs to 400 µs. The data obtained by three different techniques, namely femtosecond pump–probe optical spectroscopy, time-resolved optical absorption spectroscopy at 480 nm and transient high-field EPR spectroscopy can be summarized as follows.

1. The kinetics of ultrafast primary charge separation between the primary donor P_{700} and the primary acceptor A_0 in PS I (< 100 fs) is not affected by the

dry trehalose matrix. The spectra of the $P_{700}^{\bullet+}A_0^{\bullet-}$ radical pair in solution and in trehalose are similar.

2. The rate of $A_0^{\bullet-}$ to A_1 ET in trehalose remains similar to that in solution (lifetime ~ 27 ps), however this reaction is completed in only ~ 80% of PS I complexes, while in the remaining ~ 20% the forward reaction is prevented by the recombination of $P_{700}^{\bullet+}A_0^{\bullet-}$.

3. The forward ET from the reduced phylloquinone acceptor $A_{1A}^{\bullet-}$ in the predominant A-branch to the iron–sulfur cluster F_X slows from ~ 220 ns in solution to ~ 13 µs in trehalose, while forward ET from $A_{1B}^{\bullet-}$ in the B-branch to F_X slows significantly less, from ~ 20 ns to 30 to 80 ns.

4. As we have recently shown [30], incorporation of PS I into dry trehalose matrix leads to the prevention of forward ET reactions from $A_1^{\bullet-}$ to F_X and further to F_A/F_B in a fraction of PS I, and to the simultaneous appearance of $P_{700}^{\bullet+}A_{1A}^{\bullet-}$ recombination (lifetime ~ 130 µs). In this work we confirm this observation and also reveal the faster recombination of the $P_{700}^{\bullet+}A_{1B}^{\bullet-}$ ion-radical pair (lifetime 14 µs) in ~ 20% of the PS I complexes.

The model put forward for the effects of a trehalose glassy matrix on ET in PS I depicts the protein as being locked into several different microstates, wherein ET is blocked at various points by altering either the redox potential of the cofactors, and/or the distance between them. The results of this study support this model, as indirect measurements of one specific cofactor suggest a mixed population, wherein some fraction participates in forward ET while a smaller fraction participates in charge recombination. Additionally, the RT PS I trehalose glassy matrix appear to reasonably mimic their low temperature counterparts, particularly for kinetic phases with a strong temperature dependence.

References

1. J. H. Golbeck and D. A. Bryant, in: Curr. Top. Bioenerg, vol. 16, (Ed. C. P. Lee), Academic Press, San Diego (1991), P. 83.
2. P. Jordan, P. Fromme, H. T. Witt, O. Klukas, W. Saenger, and N. Krauss, Nature **411** (2001) 909.
3. M. Guergova-Kuras, B. Boudreaux, A. Joliot, P. Joliot, and K. Redding, Proc. Natl. Acad. Sci. USA. **98** (2001) 4437.
4. S. Santabarbara, P. Heathcote, and M. C. W. Evans, Biochim. Biophys. Acta. **1708** (2005) 283.
5. N. Srinivasan and J. H. Golbeck, Biochim. Biophys. Acta. **1787** (2009) 1057.
6. J. Sun, S. Hao, M. Radle, W. Xu, I. Shelaev, V. Nadtochenko, V. Shuvalov, A. Semenov, H. Gordon, A. van der Est, and J. H. Golbeck, Biochim. Biophys. Acta. **1837** (2014) 1362.
7. G. E. Milanovsky, V. V. Ptushenko, J. H. Golbeck, A. Y. Semenov, and D. A. Cherepanov, Biochim. Biophys. Acta. **1837** (2014) 1472.
8. H. Makita and G. Hastings, Febs Lett. **589** (2015) 1412.
9. I. V. Shelaev, F. E. Gostev, M. D. Mamedov, O. M. Sarkisov, V. A. Nadtochenko, V. A. Shuvalov and A. Y. Semenov, Biochim. Biophys. Acta. **1797** (2010) 1410.
10. S. Savikhin, W. Xu, P. Martinsson, P. R. Chitnis, and W. S. Struve, Biochem. **40** (2001) 9282.
11. K. Brettel, Febs Lett. **239** (1988) 93.
12. P. Setif and H. Bottin, Biochem. **28** (1989) 2689.
13. R. Agalarov and K. Brettel, Biochim. Biophys. Acta. **1604** (2003) 7.
14. I. R. Vassiliev, Y. S. Jung, M. D. Mamedov, A. Y. Semenov and J. H. Golbeck, Biophys. J. **72** (1997) 301.
15. K. Brettel and W. Leibl, Biochim. Biophys. Acta. **1507** (2001) 100.
16. J. F. Carpenter, L. M. Crowe and J. H. Crowe, Biochim. Biophys. Acta. **923** (1987) 109.
17. E. C. Lopez-Diez and S. Bone, Biochim. Biophys. Acta. **1673** (2004) 139.
18. N. K. Jain and I. Roy, Protein Sci. **18** (2009) 24.
19. S. Ohtake and Y. J. Wang, J. Pharm. Sci. **100** (2011) 2020.
20. J. H. Crowe, J. F. Carpenter and L. M. Crowe, Ann. Rev. Physiol. **60** (1998) 73.
21. L. M. Crowe, Comp. Biochem. Physiol. A Mol. Integr. Physiol. **131** (2002) 505.
22. G. Palazzo, A. Mallardi, A. Hochkoeppler, L. Cordone and G. Venturoli, Biophys. J. **82** (2002) 558.
23. F. Francia, M. Dezi, A. Mallardi, G. Palazzo, L. Cordone, and G. Venturoli, J. Am. Chem. Soc. **130** (2008) 10240.
24. F. Francia, G. Palazzo, A. Mallardi, L. Cordone, and G. Venturoli, Biophys. J. **85** (2003) 2760.
25. F. Francia, G. Palazzo, A. Mallardi, L. Cordone, and G. Venturoli, Biochim. Biophys. Acta. **1658** (2004) 50.
26. D. Kleinfeld, M. Y. Okamura, and G. Feher, Biochem. **23** (1984) 5780.
27. B. H. McMahon, J. D. Muller, C. A. Wraight, and G. U. Nienhaus, Biophys. J. **74** (1998) 2567.
28. L. Cordone, G. Cottone, A. Cupane, A. Emanuele, S. Giuffrida, and M. Levantino, Curr. Org. Chem. **19** (2015) 1684.
29. L. Cordone, G. Cottone, S. Giuffrida, G. Palazzo, G. Venturoli, and C. Viappiani, Biochim. Biophys. Acta. **1749** (2005) 252.
30. M. Malferrari, A. Savitsky, M. D. Mamedov, G. E. Milanovsky, W. Lubitz, K. Möbius, A. Y. Semenov, and G. Venturoli, Biochim. Biophys. Acta. **1857** (2016) 1440.
31. E. Schlodder, K. Falkenberg, M. Gergeleit, and K. Brettel, Biochem. **37** (1998) 9466.
32. G. Z. Shen, J. D. Zhao, S. K. Reimer, M. L. Antonkine, Q. Cai, S. M. Weiland, J. H. Golbeck, and D. A. Bryant, J. Biol. Chem. **277** (2002) 20343.

33. D. I. Arnon, Plant Physiol. **24** (1949) 1.
34. M. Malferrari, A. Nalepa, G. Venturoli, F. Francia, W. Lubitz, K. Möbius, and A. Savitsky, Phys. Chem. Chem. Phys. **16** (2014) 9831.
35. M. Malferrari, F. Francia, and G. Venturoli, J. Phys. Chem. B. **119** (2015) 13600.
36. L. Greenspan, J. Res. Natl. Stand. Sec. A. **81** (1977) 89.
37. S. A. Kovalenko, A. L. Dobryakov, J. Ruthmann, and N. P. Ernsting, Phys. Rev. A. **59** (1999) 2369.
38. I. V. Shelaev, F. E. Gostev, M. I. Vishnev, A. Y. Shkuropatov, V. V. Ptushenko, M. D. Mamedov, O. M. Sarkisov, V. A. Nadtochenko, A. Y. Semenov, and V. A. Shuvalov, J. Photochem. Photobiol. B. **104** (2011) 44.
39. A. L. Dobryakov, J. L. P. Lustres, S. A. Kovalenko, and N. P. Ernsting, Chem. Phys. **347** (2008) 127.
40. S. W. Provencher, Comput. Phys. Commun. **27** (1982) 229.
41. K. Möbius, A. Savitsky, A. Schnegg, M. Plato, and M. Fuchs, Phys. Chem. Chem. Phys. **7** (2005) 19.
42. V. A. Shuvalov, A. M. Nuijs, H. J. Vangorkom, H. W. J. Smit, and L. N. M. Duysens, Biochim. Biophys. Acta. **850** (1986) 319.
43. G. Hastings, F. A. M. Kleinherenbrink, S. Lin, T. J. McHugh, and R. E. Blankenship, Biochem. **33** (1994) 3193.
44. D. H. Mi, S. Lin, and R. E. Blankenship, Biochem. **38** (1999) 15231.
45. S. Savikhin and J. H. Golbeck, in: *Advances in Photosynthesis and Respiration: The Light-Driven Plastocyanin: Ferredoxin Oxidoreductase*, (Ed. J. H. Golbeck) Springer, Dordrecht (2006), P. 155.
46. C. Ruckebusch, S. Aloise, L. Blanchet, J. P. Huvenne, and G. Buntinx, Chemometr. Intell. Lab. **91** (2008) 17.
47. P. Joliot and A. Joliot, Biochem. **38** (1999) 11130.
48. P. Setif, H. Bottin, and P. Mathis, Biochim. Biophys. Acta. **808** (1985) 112.
49. A. K. Salikhov, Y. N. Molin, R. Z. Sagdeev, and A. L. Buchachenko, Spin Polarization and Magnetic Effects in Chemical Reactions, Elsevier, Amsterdam (1984).
50. K. M. Salikhov, C. H. Bock, and D. Stehlik, Appl. Magn. Reson. **1** (1990) 195.
51. K. M. Salikhov, Y. E. Kandrashkin, and A. K. Salikhov, Appl. Magn. Reson. **3** (1992) 199.
52. K. M. Salikhov, J. Schlüpmann, M. Plato, and K. Möbius, Chem. Phys. **215** (1997) 23.
53. A. J. Hoff, Q. Rev. Biophys. **17** (1984) 153.
54. D. Stehlik, C. H. Bock, and J. Petersen, J. Phys. Chem. **93** (1989) 1612.
55. P. J. Hore, in: *Advanced EPR. Applications in Biology and Biochem*, (Ed. A. J. Hoff) Elsevier, Amsterdam (1989), P. 405.
56. S. S. Eaton and G. R. Eaton, in: *Biological Magnetic Resonance*, (Eds. L. J. Berliner, S. S. Eaton, and G. R. Eaton) Kluwer/Plenum, New York (2000), P. 24.
57. I. Sieckmann, K. Brettel, C. Bock, A. Vanderest, and D. Stehlik, Biochem. **32** (1993) 4842.
58. D. E. Budil and M. C. Thurnauer, Biochim. Biophys. Acta. **1057** (1991) 1.
59. A. Savitsky, O. Gopta, M. Mamedov, J. H. Golbeck, A. Tikhonov, K. Möbius, and A. Semenov, Appl. Magn. Reson. **37** (2010) 85.